Mon. Not. R. Astron. Soc. **000**, 000–000 (0000) Printed 11 July 2007 (MN LATEX style file v2.2)

Unifying B2 radio galaxies with BL Lac objects

M.J. Hardcastle[1⋆], D.M. Worrall[1,2], M. Birkinshaw[1,2] and C.M. Canosa[1]†
[1] *Department of Physics, University of Bristol, Tyndall Avenue, Bristol BS8 1TL*
[2] *Harvard-Smithsonian Center for Astrophysics, 60 Garden Street, Cambridge, MA 02138, U.S.A.*

11 July 2007

ABSTRACT
In an earlier paper we presented nuclear X-ray flux densities, measured with *ROSAT*, for the B2 bright sample of nearby low-luminosity radio galaxies. In this paper we construct a nuclear X-ray luminosity function for the B2 radio galaxies, and discuss the consequences of our results for models in which such radio galaxies are the parent population of BL Lac objects. Based on our observations of the B2 sample, we use Monte Carlo techniques to simulate samples of beamed radio galaxies, and use the selection criteria of existing samples of BL Lac objects to compare our simulated results to what is observed. We find that previous analytical results are not applicable since the BL Lac samples are selected on beamed flux density. A simple model in which BL Lacs are the moderately beamed ($\gamma \sim 3$) counterparts of radio galaxies, with some random dispersion (~ 0.4 decades) in the intrinsic radio-X-ray relationship, can reproduce many of the features of the radio-selected and X-ray-selected BL Lac samples, including their radio and X-ray luminosity functions and the distributions of their radio-to-X-ray spectral indices. In contrast, models in which the X-ray and radio emission have systematically different beaming parameters cannot reproduce important features of the radio-galaxy and BL Lac populations, and recently proposed models in which the radio-to-X-ray spectral index is a function of source luminosity cannot in themselves account for the differences in the slopes of the radio and X-ray-selected BL Lac luminosity functions. The redshift distribution and number counts of the X-ray-selected EMSS sample are well reproduced by our best models, supporting a picture in which these objects are beamed FRI radio galaxies with intrinsic luminosities similar to those of the B2 sample. However, we cannot match the redshift distribution of the radio-selected 1-Jy sample, and it is likely that a population of FRII radio galaxies is responsible for the high-redshift objects in this sample, in agreement with previously reported results on the sample's radio and optical-emission-line properties.

Key words: galaxies: active – X-rays: galaxies – BL Lacertae objects: general – galaxies: jets

1 INTRODUCTION

The extreme properties of BL Lac objects are explained in terms of relativistic beaming of the emission from a jet oriented close to the line of sight. This model implies the existence of a substantial 'parent population' of sources whose jets are less favourably aligned, and it is widely accepted that this is the population of low-power radio galaxies (Browne 1983; Urry & Padovani 1995). Properties which are isotropic and unaffected by beaming should be similar in BL Lac objects and low-power radio galaxies. This is broadly supported by observations of extended radio emission (e.g., Antonucci & Ulvestad 1985, Kollgaard et al. 1992, Perlman & Stocke 1993, 1994), host galaxies (e.g., Ulrich 1989, Abraham, McHardy & Crawford 1991; Wurtz, Stocke & Yee 1996; Falomo 1996) and cluster environments (Pesce, Falomo & Treves 1995; Smith, O'Dea & Baum 1995; Wurtz, Stocke & Ellingson 1997).

In a series of papers (Padovani & Urry 1990; Padovani & Urry 1991; Urry, Padovani & Stickel 1991), Urry and co-workers made this model quantitative by predicting the luminosity function of BL Lac objects based on that of radio galaxies. They used the analysis of Urry & Schafer (1984) and Urry & Padovani (1991) to calculate the expected luminosity function of a population of beamed objects given a parent (unbeamed) luminosity function. With the data on radio-galaxy and BL Lac populations then available they were able to show reasonable agreement between the predictions of the model and the observed luminosity functions. They found that the luminosity function of radio-selected BL Lac objects from the 1-Jy sample (Stickel et al. 1991) was consistent with that of radio galaxies from the 2-Jy sample (Wall & Peacock 1985) if the radio-emitting plasma in the cores had a bulk Lorentz factor $\gamma_{\rm radio} > 5$. The X-

⋆ E-mail: m.hardcastle@bristol.ac.uk.
† Present address: British Telecommunications plc, PP D007, North Star House, North Star Avenue, Swindon, Wiltshire, SN2 1BS

ray luminosity function and number counts of X-ray selected BL Lac objects were consistent with the luminosity function of FRI radio galaxies observed with *Einstein* by Fabbiano et al. (1984) if the X-ray emitting plasma has a somewhat lower bulk Lorentz factor, $\gamma_{\rm Xray} \approx 3$.

The issue of the relationship between radio galaxies and X-ray and radio-selected BL Lac objects is only partially resolved by this work. The best-studied sample of X-ray selected BL Lacs is the EMSS sample (Wolter et al. 1991, Rector et al. 2000) and the best radio-selected sample is the 1-Jy sample (Stickel et al. 1991, Rector & Stocke 2001). When these samples are compared, a number of differences emerge. Some – perhaps as many as half – of the 1-Jy objects have radio structures, luminosities and emission-line properties similar to those of FRII radio galaxies (Antonucci & Ulvestad 1984, Kollgaard et al. 1992, Rector & Stocke 2001) while the EMSS BL Lacs are all FRI-like (Perlman & Stocke 1993). The luminosity functions of the two samples are also different; the radio-selected objects show evidence for positive evolution (i.e. sources were more numerous or more powerful at higher redshift) while X-ray-selected sources appear to be *negatively* evolving. Urry et al. were forced by the data then available to use an X-ray-selected sample of BL Lacs for their comparison with the X-ray luminosity function of radio galaxies, and a radio-selected sample when considering the radio luminosity function. They were thus unable to say anything about the relation between radio galaxies and the two BL Lac populations.

Radio-selected BL Lacs are often considered to be more extreme than X-ray selected objects; they have more prominent radio cores (Perlman & Stocke 1993, Laurent-Muehleisen et al. 1993, Rector & Stocke 2001), higher optical polarization with less stable position angle (Jannuzi, Smith & Elston 1994) and a lower optical starlight fraction (Stocke et al. 1985). On the other hand, their environments and host galaxies are similar to X-ray selected sources (Wurtz, Stocke & Yee 1996, Wurtz et al. 1997). This has led to suggestions that radio-selected objects are more strongly affected by Doppler boosting than X-ray selected objects, and so are being observed at smaller angles to the line of sight. Since radio-selected and X-ray selected objects have similar X-ray luminosities, this requires that the X-ray-emitting regions be less strongly beamed, or even isotropic (Maraschi et al. 1986; Celotti et al. 1993); the idea of weaker beaming is consistent with the difference in the Doppler beaming factors found by Urry et al. (1991). This in turn implies that X-ray-selected BL Lacs should be the more numerous population, since they can be seen at larger angles to the line of sight, which Celotti et al. (1993) argue is consistent with the X-ray luminosity functions of the two populations. Models of this kind can either rely on differences in velocity between X-ray and radio-emitting regions (e.g., Ghisellini & Maraschi 1989) or differences in opening angle of the jet (Celotti et al. 1993). However, these models do not account for the differences in evolutionary properties between the two samples. In section 5.4.3 of this paper we shall discuss whether they are consistent with observations of radio galaxies and with the X-ray and radio luminosity functions of the two classes.

A description of BL Lac objects in terms of the selection waveband does not necessarily reflect the underlying physics. An alternative approach is to refer to high-energy peaked BL Lacs (HBL) and low-energy peaked BL Lacs (LBL) (e.g., Giommi & Padovani 1994, Padovani & Giommi 1995), distinguishing between the two classes by their radio/X-ray flux ratios; a typical dividing line is that HBL have $\log_{10}(F_{1\ \rm kev}/F_{5\ \rm GHz}) > -5.5$, or, equivalently, $\alpha_{\rm RX} < 0.72$, where α is defined here and throughout the paper in the sense $F \propto \nu^{-\alpha}$ and $\alpha_{\rm RX}$ denotes the radio-to-X-ray two-point spectral index. By selecting bright sources at one or the other waveband we may simply be picking up objects with extreme radio/X-ray flux ratios, which suggests various possible schemes for unifying the two populations (e.g., Giommi & Padovani 1994, Fossati et al. 1997) and is consistent with the discovery of 'intermediate' BL Lacs in deeper surveys (Laurent-Muehleisen et al. 1999). From multi-wavelength observations it has been found that the spectral energy distributions (SEDs) of BL Lacs can be represented by a low-frequency peak (assumed to be synchrotron radiation) and a high-frequency peak (perhaps inverse-Compton radiation). There is evidence that the positions of these peaks shift to higher frequencies at lower bolometric luminosities (Sambruna, Maraschi & Urry 1996, Fossati et al. 1998). However, Giommi, Menna & Padovani (1999) do not find the increase in the numbers of HBL at fainter radio fluxes that is expected in such a model.

To try to resolve some of the outstanding issues in BL Lac unification it is productive to learn more about the presumed parent population of many or all of the BL Lac objects, namely the low-power radio galaxies. Work to date has been hampered by the lack of a well-defined, low-frequency-selected sample of radio galaxies with well-known radio and X-ray properties. In a previous paper (Canosa et al. 1999) we presented results for the 40 members ($\approx$ 80 per cent) of the B2 bright sample of radio galaxies which had been observed in pointed *ROSAT* observations. The high spatial resolution of *ROSAT* allowed us to separate the nuclear emission from extended emission due to the hot-gas environment of the radio source. In this paper we use these data to derive a new X-ray luminosity function for the nuclei of B2 radio sources, largely free from contamination from thermal emission from the sources' hot-gas environments. We use numerical techniques to extend earlier work, first asking how well a simple beaming model can be used to link the X-ray and radio luminosity functions of radio galaxies, and then investigating the expected relationship between radio galaxies and BL Lac objects when selection bias is taken into account.

Throughout the paper we use a cosmology in which $H_0 = 50\ {\rm km\,s^{-1}\,Mpc^{-1}}$ and $q_0 = 0$.

2 LUMINOSITY FUNCTIONS OF B2 BRIGHT GALAXIES

The B2 bright sample, described by Colla et al. (1975), consists of 52 radio sources with 408-MHz radio flux $\gtrsim 0.20$ Jy identified with galaxies with photographic magnitudes $\lesssim 15.6$. (The flux limit is declination-dependent; see Colla et al. for details.) The sample is flux-complete for all but the largest sources. The sky coverage of the sample is 1.154 sr [cf. Colla (1975); the figure quoted by Ulrich (1989) appears to be in error]. Of the 52 objects in the sample, two (B2 0207+38 and 1318+34) are starburst galaxies, and will not be considered further in this paper. One (B2 1833+32) is the broad-line FRII radio galaxy 3C 382, which we also exclude from further consideration because FRII radio sources do not participate in most radio galaxy-BL Lac unification models, and two (B2 1101+38 and 1652+39) are the well-known BL Lac objects Mrk 421 and Mrk 501, which we did not discuss in Canosa et al. (1999), but which will be included in the sample we discuss here in order that it should be unbiased with respect to orientation[1]. The remainder are more

[1] We have obtained X-ray flux densities for these objects from archival *ROSAT* data, in order to match our analysis of the radio galaxies. For Mrk

or less typical FRI radio sources, though the sample includes some peculiar objects such as B2 1626+39 (3C 338). Ulrich (1989) has shown that the B2 bright sample is well matched in *unbeamed* properties, like extended radio luminosity, to samples of nearby BL Lac objects.

Because an unbiased selection on unbeamed properties is important, we need to consider whether some of the sample sources exceed the 408-MHz flux limit solely because of a beamed radio component. We may estimate this by subtracting the 5-GHz core flux density from the total 408-MHz flux, on the assumption that the core spectrum is flat between these two frequencies, and seeing whether the result lies below the B2 position-dependent flux limit. On this basis, 4 sources (B2 0648+27, 1108+27, 1144+35 and 1553+24) possibly have too low a 408-MHz flux to be in the sample through extended emission alone. Of these, the core of 1144+35 is known to dominate the extended structure, and to be variable (Giovannini et al. 1999). 0648+27 is also core-dominated (e.g., Antonucci 1985). We exclude these two sources from the sample. The other two are reasonably normal members of the sample which happen to lie at the flux limit, so that the case for excluding them (given the large uncertainties in core spectrum) is uncertain – Laing et al. (1999), on a similar basis, chose not to exclude these two sources from their sample of jetted objects. Our revised, unbiased sample then consists of 47 objects, whose properties are listed in Table 1. We have nuclear X-ray information for all but 8 of these.

We are now in a position to construct a luminosity function for the extended radio emission from our unbiased sample. For a source which has a detected radio core at 5 GHz, we subtract its flux density from the 408-MHz flux density before making the luminosity calculation; for sources without detected cores (where the upper limit on core flux density is typically a small fraction of the total flux density) we just use the total 408-MHz flux density, and we also do this for 1108+27 and 1553+24. For the purposes of calculating luminosities we correct the 408-MHz flux densities to the Baars et al. (1977) scale from the Kellerman (1964) scale used in B2 the catalogue (Colla et al. 1970), using the factor 1.074 suggested by Baars et al.. Spectral indices are also corrected to the Baars et al. scale in the same way. To generate a differential luminosity function we use the $1/V_{\rm max}$ method, taking into account both the optical and radio selection criteria; the optical selection criterion is the important one in 31/47 objects. The radio flux limits and flux densities used to determine $V_{\rm max}$ are the original values, without core subtraction. We assign errors to the bins in the luminosity function using the method of Wolter et al. (1994), having verified by simulation that the error estimates derived from this method are close to the real statistical errors. Our differential luminosity function for the extended flux from the sample is plotted in Fig. 1. It is consistent with the luminosity function derived for the sample by de Ruiter et al. (1990).

We can similarly derive 5-GHz and 1-keV luminosity functions for the nuclei of the sample, using the method described by Wolter et al. (1994). The values of $V_{\rm max}$ (or $V_{\rm a}$ in their notation) are derived from the selection band (i.e. the 408-MHz flux densities and optical magnitudes) while the luminosities are those in the observation band. The 5-GHz radio core flux densities include 5 upper limits; this is a sufficiently small fraction of the data that we are not going to be grossly in error if we assume that the true values of the core fluxes for these sources are equal to the limits (i.e. treat limits as detections at the limit level). Doing this leads to the luminosity function plotted in Fig. 2. (Throughout the paper we assume that the radio spectral index α of the cores is 0.)

However, the 1-keV flux densities include 12 upper limits and 8 unobserved sources. In most cases the upper limits are the result of an ambiguity in the separation of nuclear and extended X-ray emission. Since we have demonstrated that the unobserved sources have no known bias with respect to the rest of the sample (Canosa et al. 1999), we can simply scale the luminosity function computed for the other sources by a factor 47/39. But the large number of X-ray limits (nearly one third of the total observed sources), could seriously affect the derived luminosity function. To assess the effect of the limits, we computed the luminosity function in four different ways: (a) with the limits treated as detections; (b) with the non-detected sources omitted altogether and the results scaled; (c) with the limits treated as detections at 0.1 times the limit level; and (d) with the limits replaced by the values that the X-ray cores 'should' have according to the radio-X-ray core correlation reported in Canosa et al. (1999). The resulting luminosity functions were similar, with slopes and normalizations of straight-line fits to the data being consistent within the statistical uncertainties, so our results here are insensitive to the treatment of the upper limits. Accordingly, we treat the limits as detections in order to generate Fig. 3, which has also been scaled to take account of the unobserved sources. (Throughout the paper we assume that the X-ray spectral index of cores is $\alpha = 0.8$.) The result is the first nuclear X-ray luminosity function to be computed for a sample of radio galaxies.

Since the analysis of Canosa et al. (1999), we have obtained the first *Chandra* images of FRI radio galaxies from the B2 sample (Worrall et al. 2001; Hardcastle et al. 2002). These show that in some of these objects there is extended X-ray emission on scales of a few arcseconds, in addition to a point-like nucleus and the larger-scale group or cluster emission that we have discussed elsewhere (Canosa et al. 1999; Worrall & Birkinshaw 2000). This small-scale extended emission would have been unresolved to *ROSAT*, and therefore contaminates the nuclear 1-keV flux densities we quote in this paper. But it does not dominate the total soft-X-ray flux in the B2 objects we have observed with *Chandra* so far, and we know from the correlation between radio, X-ray and optical nuclear emission in these objects (Canosa et al. 1999; Hardcastle & Worrall 1999, 2000) that a significant fraction of the *ROSAT*-observed 1-keV emission must arise in a beamed nucleus. It is therefore reasonable to use the current values to test the predictions of unified models, provided we bear in mind the possible distorting effects of this contaminating extended emission.

3 LUMINOSITY FUNCTIONS FOR BL LAC OBJECTS

To test unified models using the new B2 luminosity function we must have comparison samples of BL Lac objects. The two comparison samples we shall consider in this paper are the 1-Jy sample of radio-selected BL Lacs [we use the 34-object sample of Stickel et al. (1991), because of the good availability of X-ray information, but with the redshifts tabulated by Rector & Stocke (2001)] and the EMSS sample of X-ray selected objects [we use the 41-object 'D40' sample of Rector et al. (2000)]. Flux densities are now available for almost all objects in both these samples at both 5-GHz radio and X-ray frequencies (Urry et al. 1996, Fossati et al. 1998 and references therein; Rector et al. and references therein). So, unlike Urry and co-workers, we are not limited to comparing the radio luminosity function of the B2s to the radio luminosity function of

421 there were four observations at different epochs in 1992–3, and the flux density we use corresponds to the median count rate in these observations.

Table 1. The sample of B2 radio galaxies and their properties.

B2 name	Other name	z	S_{408} (Jy)	α_{408}	$S_{5,\,\mathrm{core}}$ (mJy)	Reference	$S_{1\,\mathrm{keV},\,\mathrm{core}}$ (nJy)
0034+25		0.0321	0.29	0.63	10	1	–
0055+30	NGC 315	0.0167	3.01	0.33	450	3	190 ± 10
0055+26	NGC 326	0.0472	5.26	0.81	8.6	4	11 ± 2
0104+32	3C 31	0.0169	10.6	0.62	92	1	64 ± 7
0116+31	4C 31.04	0.0592	3.75	0.39	$<$100	7	–
0120+33	NGC 507	0.0164	0.74	1.4	1.4	1	$<$83
0149+35	NGC 708	0.0160	0.39	0.6	5	1	$<$59
0206+35	4C 35.03	0.0375	4.90	0.63	106	1	29 ± 5
0222+36		0.0327	0.37	0.21	90	1	$<$10
0258+35	NGC 1167	0.016	4.19	0.51	$<$15	1	$<$10
0326+39		0.0243	2.04	0.53	70	1	36 ± 4
0331+39	4C 39.12	0.0202	1.85	0.49	125	1	230 ± 20
0722+30		0.0191	0.41	1.08	51	1	$<$20
0755+37	NGC 2484	0.0413	6.34	0.65	190	1	85 ± 9
0800+24		0.0433	0.34	0.65	3	1	$<$3
0836+29A	4C 29.30	0.0650	1.68	0.62	8.2	1	$<$4
0844+31	4C 31.32	0.0675	4.03	0.75	58	1	–
0915+32		0.0620	0.50	0.45	8	1	–
0924+30		0.0266	1.88	1.01	$<$0.4	1	$<$20
1040+31	4C 29.41	0.036	1.82	0.59	55	1	16 ± 2
1101+38	Mrk 421	0.03	1.24	0.23	520	8	7.0×10^4
1102+30		0.0720	1.0	0.69	26	1	–
1108+27	NGC 3563	0.0331	0.21	0.45	14	2	–
1113+29	4C 29.41	0.0489	5.32	0.53	41	1	10 ± 6
1122+39	NGC 3665	0.0067	0.31	0.61	6	1	1 ± 2
1217+29	NGC 4278	0.0021	0.62	0.21	350	1	100 ± 20
1254+27	NGC 4839	0.02464	0.23	0.83	2.3	2	25 ± 6
1256+28	NGC 4869	0.0224	1.57	1.01	2	1	$<$2
1257+28	NGC 4874	0.0239	0.54	0.73	1.1	1	6 ± 2
1317+33	NGC 5098	0.0379	0.26	0.90	8	6	7 ± 4
1321+31	NGC 5127	0.0161	3.87	0.62	21	1	$<$10
1322+36	NGC 5141	0.0175	1.84	0.43	75	1	$<$10
1346+26	A 1795	0.0633	3.38	0.89	53	1	36 ± 10
1350+31	3C 293	0.0452	10.90	0.67	100	1	$<$20
1422+26		0.0370	2.17	0.71	25	1	4 ± 1
1525+29	A 2079	0.0653	0.46	0.70	2.5	1	–
1553+24		0.0426	0.21	0.25	53.6	2	28 ± 6
1610+29	NGC 6086	0.0313	0.34	0.69	$<$6	1	12 ± 3
1615+35	NGC 6109	0.0296	5.80	0.79	28	1	13 ± 2
1621+38	NGC 6137	0.031	1.00	0.53	50	1	16 ± 3
1626+39	3C 338	0.0303	19.46	1.32	100	1	20 ± 7
1652+39	Mrk 501	0.034	1.90	0.15	1420	5	1.7×10^4
1855+37		0.0552	0.9	0.81	$<$100	1	35 ± 6
2116+26		0.0164	0.34	0.02	47	1	–
2229+39	3C 449	0.0171	6.93	0.61	37	1	15 ± 5
2236+35		0.0277	0.83	0.55	8	1	14 ± 4
2335+26	3C 465	0.0301	21.7	0.75	230	1	66 ± 6

408-MHz flux densities and α_{408} (the low-frequency spectral index) have been corrected to the scale of Baars et al. (1977) as described in the text. 5-GHz flux densities for the cores are taken from the literature. References for these are as follows: (1) Giovannini et al. (1988) (2) Fanti et al. (1987) (from 1.4 GHz) (3) Venturi et al. (1993) (4) Fomalont, private communication (5) Stickel et al. (1991) (6) Measured from maps supplied by R. Morganti (7) Cotton et al. (1995) (8) Antonucci & Ulvestad (1985) (extrapolated from 1.5 GHz). 1-keV nuclear flux densities are taken from Canosa et al. (1999), except for those for Mrk 421 and 501, which are discussed in the text, and for B2 1553+24, for which Canosa et al. quoted an incorrect X-ray flux density, although the count rate they quote is correct.

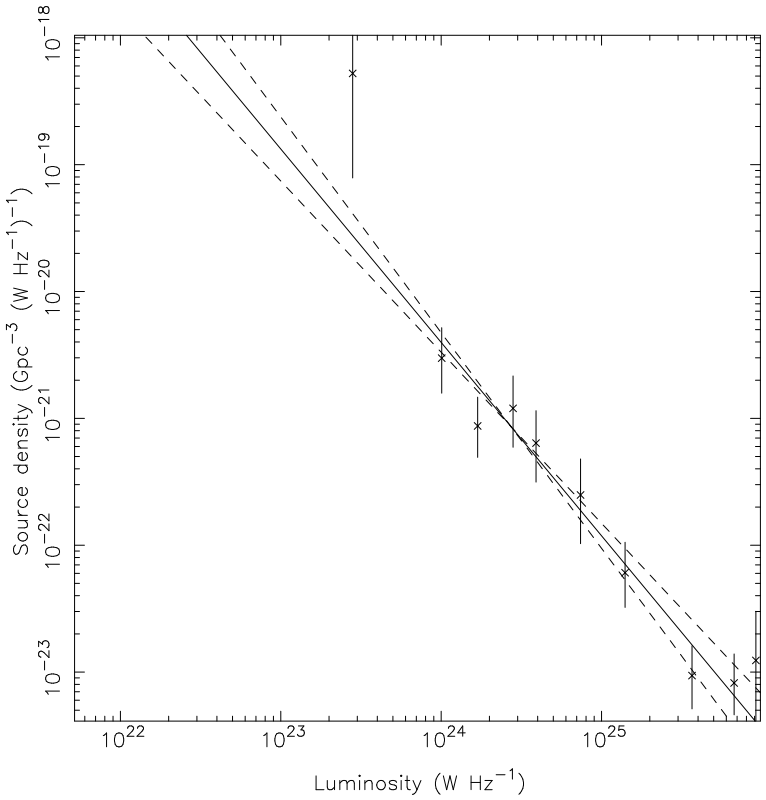

Figure 1. Differential 408-MHz luminosity function for extended flux from the B2 sample. The solid line shows the best-fit linear regression slope to the data, -1.52 ± 0.13, while the dashed lines give an indication of the 1σ error. Each bin represents 5 sources.

radio-selected BL Lacs, and so on; we can compare the luminosity functions of both kinds of BL Lac in both wavebands to the radio-galaxy observations.

Accordingly, we have constructed radio and X-ray luminosity functions for the two samples in the same way as for the radio-galaxy data. In both cases, we calculate $V_{\rm max}$ using the energy band in which the source was selected. We take account of the optical flux selection criterion for the 1-Jy sample (< 20 mag on sky survey plates; Stickel et al.1991) and the variable sensitivity of the EMSS (Gioia et al. 1990) in the manner described by Morris et al. (1991). In both cases, we include modest luminosity evolution as an exponential function of look-back time (positive for the radio-selected objects, negative for the X-ray-selected objects), in the manner described by Wolter et al. (1994), to obtain $< V/V_{\rm max} > \approx 0.5$; the effect of this assumption on the results is quite small. For the sources with only lower redshift limits, we have used the limit as though it were the actual redshift of the source. For the few sources without known redshifts (5 in the 1-Jy sample, 2 in the EMSS sample), we have used the median redshift for the detected objects in the sample from which they were drawn (0.55 for the 1-Jy sample, 0.30 for the EMSS sample). We have constructed luminosity functions on the assumption that the nuclear components in both radio and X-ray are dominant in both classes of source.

The results are plotted in Figs 2 and 3. They are, as we would expect, consistent on the whole with other determinations of the luminosity functions for these samples (e.g., Stickel et al. 1991, Wolter et al. 1994).

4 APPLICATION OF THE URRY & SCHAFER MODEL

Urry & Schafer (1984) discuss the effect of relativistic beaming on a differential luminosity function which is intrinsically a simple power law (i.e., one which has the form $\phi(L) = KL^s$, where L is the luminosity, ϕ has dimensions volume^{-1} luminosity^{-1}, and s is the slope of the luminosity function.) They show that the observed luminosity function is a broken power law. The low-luminosity slope is given by $-(p+1)/p$, where p is the power to which the Doppler factor is raised in the beaming calculation; for a jet, $p = 2 + \alpha$, where α is the jet spectral index. At high luminosities, the slope of the observed luminosity function is the same as that of the intrinsic luminosity function.

The luminosity functions for the radio and X-ray cores of the B2 objects shown in Figs 2 and 3 are for beamed components of the radio source. The unbeamed 408-MHz radio luminosity function in Fig. 1 can be treated as a single power law, since the well-known steepening (e.g., Machalski & Godlowski 2000) in the low-frequency radio source luminosity function occurs around $L_{408\rm MHz} \gtrsim 4 \times 10^{25}$ W Hz^{-1}. If we make the further assumption that the *intrinsic* core radio and X-ray fluxes of the B2s are proportional to the extended 408-MHz flux, the Urry & Schafer analysis can be applied to these data. Since most sources are at large angles to the line of sight, we are predominantly seeing the low-luminosity end of the beamed luminosity function. Urry & Schafer's result leads us to expect slopes of -1.50 and -1.36 for the 5-GHz and 1-keV core luminosity functions, respectively. The actual slopes (-1.67 ± 0.15 and -1.54 ± 0.09 respectively) are somewhat steeper than, but consistent with, these expectations, supporting our assumption above about the relationship between total luminosity and intrinsic core luminosity. Since the slope of the unbeamed, 'parent'

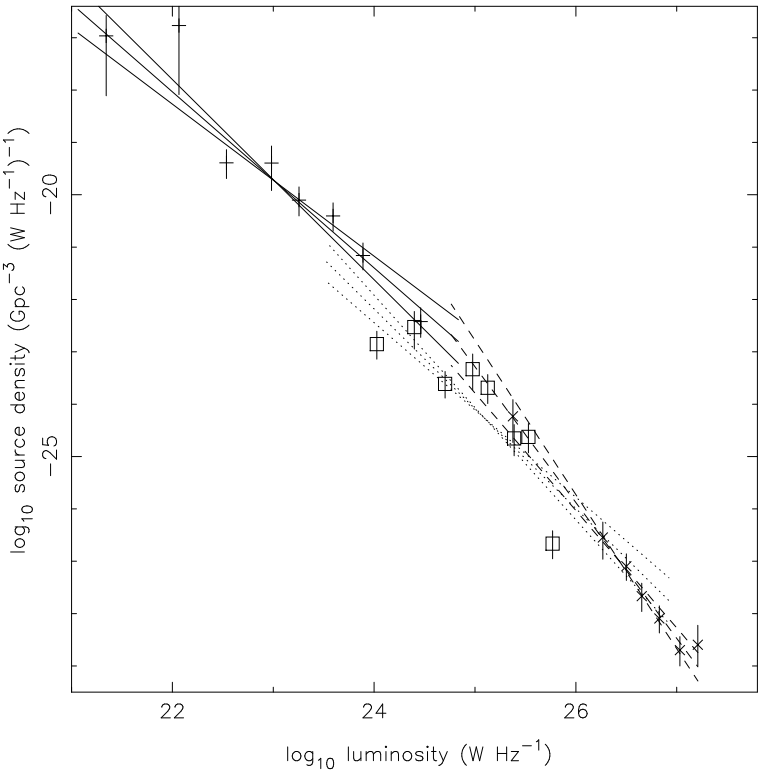

Figure 2. Differential 5-GHz core luminosity function for the B2 sample and the comparison samples of BL Lac objects. The inner lines show the best-fit linear regression slope to the data, while the two outer lines show the 1σ error. Crosses mark data points from the B2 sample, Xs the 1-Jy sample and boxes the EMSS sample, while solid lines denote fits to the B2s, dashed lines the 1-Jy sample and dotted lines the EMSS sample. The slope of the luminosity function for the B2 sample is -1.68 ± 0.16, for the 1-Jy sample -2.59 ± 0.26, and for the EMSS sample -1.91 ± 0.18. Each bin represents 5 sources.

luminosity function should be equal to that of the 408-MHz data, -1.52 ± 0.13, which is similar to the predicted slope of the beamed luminosity function, we would not expect to see a break in the slope of the beamed luminosity function at high luminosities, and indeed there is no evidence for such a break in the luminosity functions for the beamed emission from the B2s.

What would we expect to see on this model for the BL Lac samples if the B2 sources were their parent population? The BL Lac objects are clearly at the luminous end of the beamed luminosity function, and therefore we should recover the slope of the parent luminosity function. Since this is ~ 1.5, a simple application of the Urry & Schafer model would cause us to expect the slopes of the differential luminosity functions of BL Lac objects that are beamed versions of the B2 radio galaxies to be ~ 1.5 (this result is independent of the value of p). The observed slopes are much steeper than this, corresponding to a parent population with an unbeamed slope ~ 2. Since the slope of the luminosity function of higher-luminosity radio galaxies is more similar to 2, we might be able to account for this by saying that these BL Lacs are beamed versions of more luminous sources than the B2s. However, the extended radio luminosities of the BL Lacs are mostly FRI-like, and the luminosity functions in radio and X-ray of the two populations overlap. Either the B2s, in spite of these similarities, are not the parent population of these objects, or the analysis of Urry & Schafer is not applicable.

5 LUMINOSITY FUNCTIONS FROM SIMULATED OBSERVATIONS

Urry & Schafer predicted the luminosity functions of beamed populations using simple mathematical arguments. An alternative approach is to use Monte Carlo simulations to generate observations of such sources, based on the information we have on the parent population, and to generate luminosity functions from this simulated population. In this section we adopt that approach.

5.1 Models

The initial model we adopt is a simple one. Each Monte-Carlo source is assigned a low-frequency luminosity drawn from the power-law fit to the 408-MHz luminosity function of the B2 radio galaxies (Fig. 1), assuming that luminosities lie between 10^{23} and 8×10^{25} W Hz^{-1}. This luminosity range matches the B2 observations, and its lower bound is close to the lower limit on the luminosity of AGN found when the radio-galaxy luminosity function is constructed for large samples (Condon 1989; Machalski & Godlowski 2000). However, it is not clear whether the lack of radio galaxies below this luminosity indicates a real physical lower limit on radio-galaxy luminosity, or whether it simply becomes impossible to distinguish them from the much more numerous starbursts; for example, Sadler et al. (2001), using an optical approach to classification, find no sign of a turnover, with a luminosity function going as low as a few $\times 10^{22}$ W Hz^{-1} at 408 MHz. We comment below (section 5.3) on the effects on unified schemes of allowing the radio-galaxy luminosity function to extend to lower luminosities.

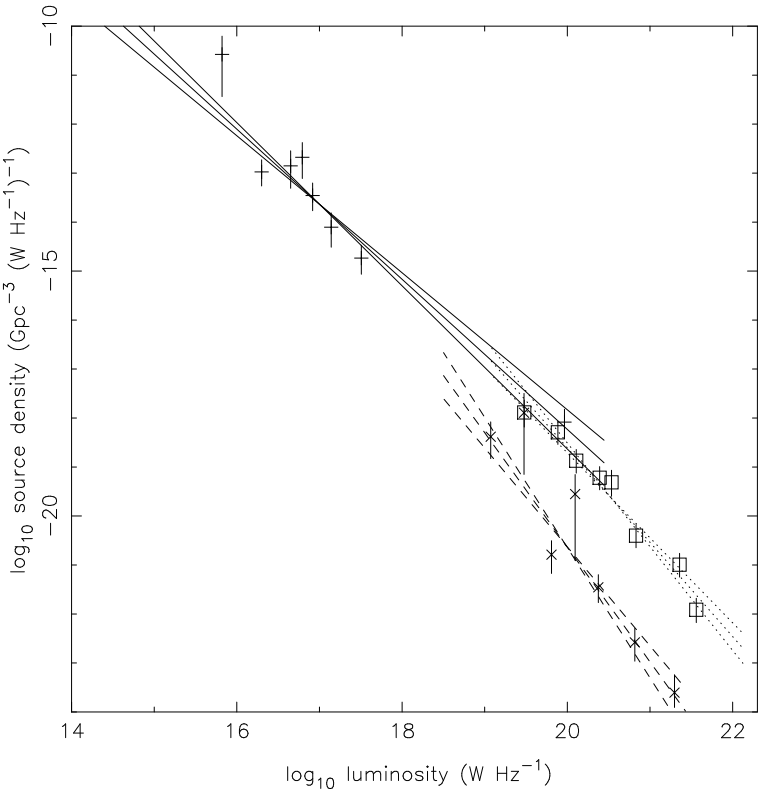

Figure 3. Differential 1-keV nuclear luminosity function for the B2 sample and the BL Lac objects. Lines and symbols are as in Fig. 2. The slope of the luminosity function for the B2 sample is -1.53 ± 0.09, for the 1-Jy sample -2.34 ± 0.21, and for the EMSS sample -1.93 ± 0.13. Each bin represents 5 sources.

The rest-frame luminosity of the core in both radio and X-rays is assumed to be a fixed fraction f of the total low-frequency luminosity; the observed core luminosity depends on f and on the beaming Lorentz factor and the (randomly chosen) angle to the line of sight. This implies that the ratio of core luminosity to extended luminosity, known as the 'core prominence', for a given source is a function only of the Doppler factor $\mathcal{D} = [\gamma(1-\beta\cos\theta)]^{-1}$, where γ is the Lorentz factor, $\beta = (1-1/\gamma^2)^{1/2}$, and θ is the angle to the line of sight and of the 'intrinsic prominence', the core prominence in its rest frame. This simple model has been used previously to constrain core Lorentz factors (e.g., Morganti et al. 1995; Hardcastle et al. 1999). Later we will consider the effects of introducing some dispersion into the relation between rest-frame core and total low-frequency luminosity.

To use this model to generate luminosity functions, we need to constrain f and γ. We do this by examining the distribution of radio and X-ray core prominences in the B2 sample, using the total 408-MHz luminosity as the normalizing quantity. This dispersion is quite broad in both bands (Fig. 4), so that large values of γ are required. We use the approach of Hardcastle et al. (1999), who used the K-S test to investigate the consistency between the probability distribution implied by the data and that of a beaming model for a given value of γ and intrinsic prominence. For the Lorentz factors ($\gamma \gtrsim 2$) required from observations of superluminal motion in BL Lac objects, fitting in small samples results in a degeneracy between f and γ; typically, the best-fitting values are constrained to lie along a line in f-γ space which can be shown, by integrating the Doppler beaming expression over all angles, to be

$$f\left\{\gamma\left[\frac{1-(1-1/\gamma^2)^{1/2}}{2}\right]\right\}^{-(2+\alpha)} \approx \bar{f}_{\rm o}$$

where $\bar{f}_{\rm o}$ is the mean observed prominence at the frequency of interest. Only with samples of $\gg 100$ sources could there be enough sources in the highly beamed tail of the distribution to set upper and lower limits on γ. Using the present sample, we find that the data are best fit with $\gamma \gtrsim 2.5$ for both the radio and X-ray. In what follows, we choose values of γ which obey this constraint, and corresponding values of f derived from our fits.

5.2 Simulation

We simulated observations of BL Lac sources with sky coverage and flux limits similar to those of the real samples. We began by generating samples matched to the B2 sample itself; we verified that we obtained 408-MHz, 5-GHz and 1-keV luminosity functions which were consistent with the observations (and with the analytical results of Urry & Schafer) and that the luminosity functions obtained were unaffected if we extended the range of simulated luminosity beyond that observed in the B2 sample. To simulate the optical magnitude limit, we assigned optical absolute magnitudes to the simulated sources based on their radio luminosities and the observed weak correlation between radio luminosity and absolute magnitude. Next we simulated 1-Jy and EMSS samples. The simulated 1-Jy sample was selected on the basis of radio core flux density and did not use the optical magnitude limit of the real sample; this is acceptable, since the optical limit in the real data only dominates the $V_{\rm max}$ calculation in 3/34 objects. The simulated EMSS sample was selected on X-ray core flux density and included the ef-

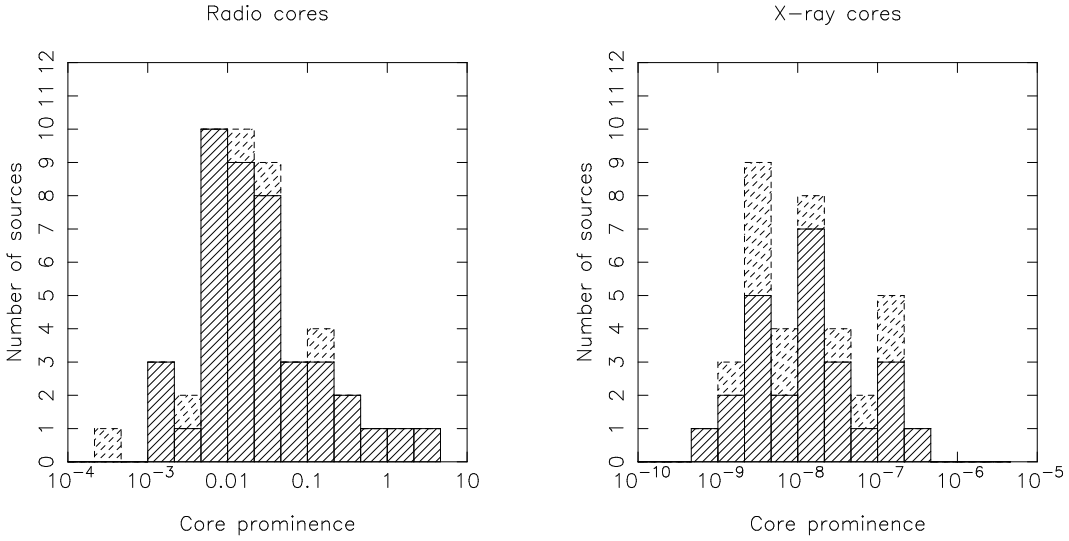

Figure 4. Radio and X-ray core prominence for the B2 bright sample, defined as discussed in the text. Dashed boxes denote upper limits on prominence.

fects of the variable sensitivity of the EMSS. In both cases, we assume that all objects which meet the flux density selection criterion are BL Lac objects, given that they have been generated from the B2 parent population and that they are all strongly core-dominated as a result of the selection criterion (we find that, even for the lowest γ values, almost all the selected objects are more strongly core-dominated than the simulated or real B2 sources, which of course include some BL Lac objects themselves, and that their core prominences at 5 GHz are comparable to those of real BL Lac objects). This assumption may be an important source of error in the simulations, and we return to it below (section 6). We also assume no evolution in the FRI parent population, since the amount of evolution is known to be small at low redshifts. We discuss the possible effects of evolution in section 6.

Several interesting results emerge from these simulations. Most strikingly, the slopes of the simulated core luminosity functions for both radio- and X-ray selected objects are systematically steeper than the values predicted by the models of Urry & Schafer, and more consistent with the measured slopes (Figs 2 and 3). It appears that the analysis of Urry & Schafer does not apply *if the beamed sample is selected on beamed rather than unbeamed flux*; it is only applicable if the selection flux is unbeamed (as for the B2 objects).

5.3 Matching observations

We can now try to vary the parameters of these simulations to obtain a better match to the observed data. There are several features of the observed samples which we would like our simulated samples to match, including:

(i) the total number of sources
(ii) the slope and range of the luminosity functions
(iii) the redshift distribution, and
(iv) the distribution of $\alpha_{\rm RX}$.

In what follows we concentrate on reproducing the 5-GHz radio luminosity functions, as the data in this waveband have smaller uncertainties than the X-ray data and are less strongly affected by factors such as variability. The inputs we are using necessarily make the simulated B2 sample match the data on criteria (i), (ii) and (iii), and this match is relatively insensitive to beaming parameters, since the B2s are not selected on beamed emission. The simulated luminosity functions for both X-ray and radio-selected BL Lac objects in our models overlap with the luminosity function for the (simulated) B2 objects, as in the real data. The degree to which they overlap in luminosity, and the number of sources in the simulated BL Lac samples, is quite a strong function of the beaming Lorentz factor γ (and its associated f values). For $\gamma = 3$, the simulations slightly underpredict the observed numbers of sources in both BL Lac samples (Table 2), and they also predict considerably lower minimum and maximum luminosities than are observed. With $\gamma = 5$, we over-predict the observed numbers of sources, but do a better job of predicting their luminosity bounds. The best results come from simulations with intermediate values of γ, for example $\gamma = 3.5$ (Fig. 5). This simulation predicts approximately the right total number of BL Lacs in the two surveys, and it also matches the luminosity range and the slope of the luminosity function, so that criteria (i) and (ii) are satisfied. It does not produce enough high-luminosity, high-redshift 1-Jy BL Lac objects, so that we cannot claim to have satisfied criterion (iii) for this sample; the redshift distributions of the real and simulated data are shown in Fig. 6. However, it is known that at least some of the 1-Jy sample are too luminous in extended emission to be FRIs and have FRII-like radio structure; such objects cannot be generated in our simulations. Criterion (iii) seems to be satisfied for the simulated EMSS samples (Fig. 6).

The numbers of BL Lacs produced in the simulations do not depend very strongly on the adopted lower limit on the total. This tells us that relatively few of the simulated BL Lac objects come from intrinsically low-luminosity radio galaxies, on the reasonable assumption that these objects do not have more strongly beamed cores than the B2s. This lends support to the idea that the B2 radio galaxies (together, in the case of the 1-Jy radio sources, with more luminous radio galaxies) are indeed representative of the parent population for these samples.

These simulations fail to reproduce the observed distinction between the luminosity functions of the X-ray and radio-selected BL Lac objects. This is not surprising: in the model we have considered so far, the radio and X-ray cores are both a fixed fraction of the total low-frequency luminosity, with the result that selection in

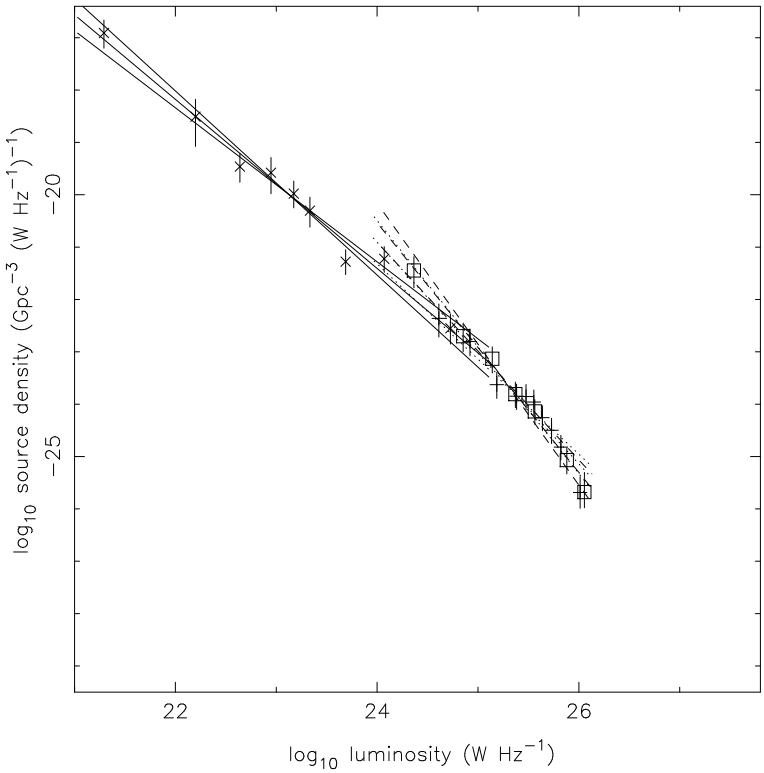

Figure 5. Simulated 5-GHz core luminosity function for B2 radio galaxies, 1-Jy BL Lac objects and EMSS BL Lac objects with $\gamma = 3.5$. The symbols and scale match those of Fig. 2.

Table 2. Some results of the simulations for different model parameters

Model	Simulated B2 sample			Simulated 1-Jy sample			Simulated EMSS sample		
	Number	Slope	Intercept	Number	Slope	Intercept	Number	Slope	Intercept
$\gamma = 3$, no scatter	55 (6)	-1.53 (0.10)	15.4 (2.2)	21 (3)	-2.40 (0.24)	37.0 (6.1)	32 (6)	-2.36 (0.25)	35.9 (6.4)
$\gamma = 3.5$, no scatter	54 (7)	-1.53 (0.10)	15.3 (2.3)	35 (5)	-2.28 (0.15)	34.1 (3.9)	60 (6)	-2.16 (0.13)	31.0 (3.3)
$\gamma = 5$, no scatter	57 (7)	-1.45 (0.09)	13.5 (2.0)	144 (13)	-2.07 (0.05)	29.2 (1.2)	203 (14)	-1.99 (0.06)	26.9 (1.6)
$\gamma = 3.0$, 0.25 dex scatter	55 (8)	-1.49 (0.12)	14.4 (2.8)	29 (6)	-2.54 (0.22)	40.5 (5.7)	42 (5)	-2.31 (0.24)	34.5 (6.0)
$\gamma = 3.0$, 0.4 dex scatter	58 (5)	-1.48 (0.11)	14.2 (2.4)	53 (5)	-2.45 (0.13)	38.5 (3.2)	55 (8)	-1.96 (0.14)	25.6 (3.6)
$\gamma = 3.0$, 0.5 dex scatter	56 (6)	-1.45 (0.13)	13.5 (3.1)	80 (9)	-2.38 (0.06)	36.9 (1.6)	75 (8)	-1.88 (0.20)	23.4 (5.1)
$\gamma = 3.5$, 0.25 dex scatter	56 (9)	-1.44 (0.09)	13.4 (2.1)	51 (6)	-2.36 (0.10)	36.2 (2.5)	78 (9)	-2.03 (0.18)	27.7 (4.5)
$\gamma = 3.5$, 0.4 dex scatter	53 (6)	-1.39 (0.09)	12.0 (2.1)	86 (10)	-2.35 (0.05)	36.1 (1.3)	98 (7)	-1.87 (0.14)	23.5 (3.5)
$\gamma = 3.5$, 0.5 dex scatter	55 (5)	-1.40 (0.06)	12.4 (1.5)	136 (12)	-2.29 (0.05)	34.7 (1.3)	124 (13)	-1.77 (0.19)	20.8 (4.7)
$\gamma = 3.5$, luminosity-dependent $\alpha_{\rm RX}$	57 (6)	-1.48 (0.13)	14.3 (2.9)	35 (7)	-2.29 (0.10)	34.3 (2.5)	783 (27)	-1.79 (0.03)	21.5 (0.7)

Details of the models used are given in the text. For each model the mean result of a number of simulations is quoted, together with the standard deviation of that parameter in parentheses. Slopes and intercepts are for the radio luminosity function only; the intercept is in units of $\log_{10}({\rm Gpc}^{-3}\ {\rm W}^{-1}\ {\rm Hz})$. Since the B2 objects are selected on unbeamed flux, their numbers in simulated samples are expected to be independent of beaming parameters, and are included here for completeness only. These results are insensitive to the choice of cosmological parameters. For comparison, the total numbers of B2, 1-Jy and EMSS objects in the real data are 47, 34, and 41 respectively, and the slopes of their radio core luminosity functions are -1.68 ± 0.16, -2.59 ± 0.26, and -1.91 ± 0.18 respectively.

the radio is effectively identical to selection in the X-ray. In other words, the radio-to-X-ray spectral index of the simulated sources, $\alpha_{\rm RX}$, is approximately fixed, which is unrealistic. Fig. 7 shows the distribution of $\alpha_{\rm RX}$ for the real and simulated data. Criterion (iv) is not met either for the simulated B2s or for the simulated BL Lac samples. In the next section of the paper we discuss ways of reproducing the observed differences in the slopes of the luminosity functions in different bands.

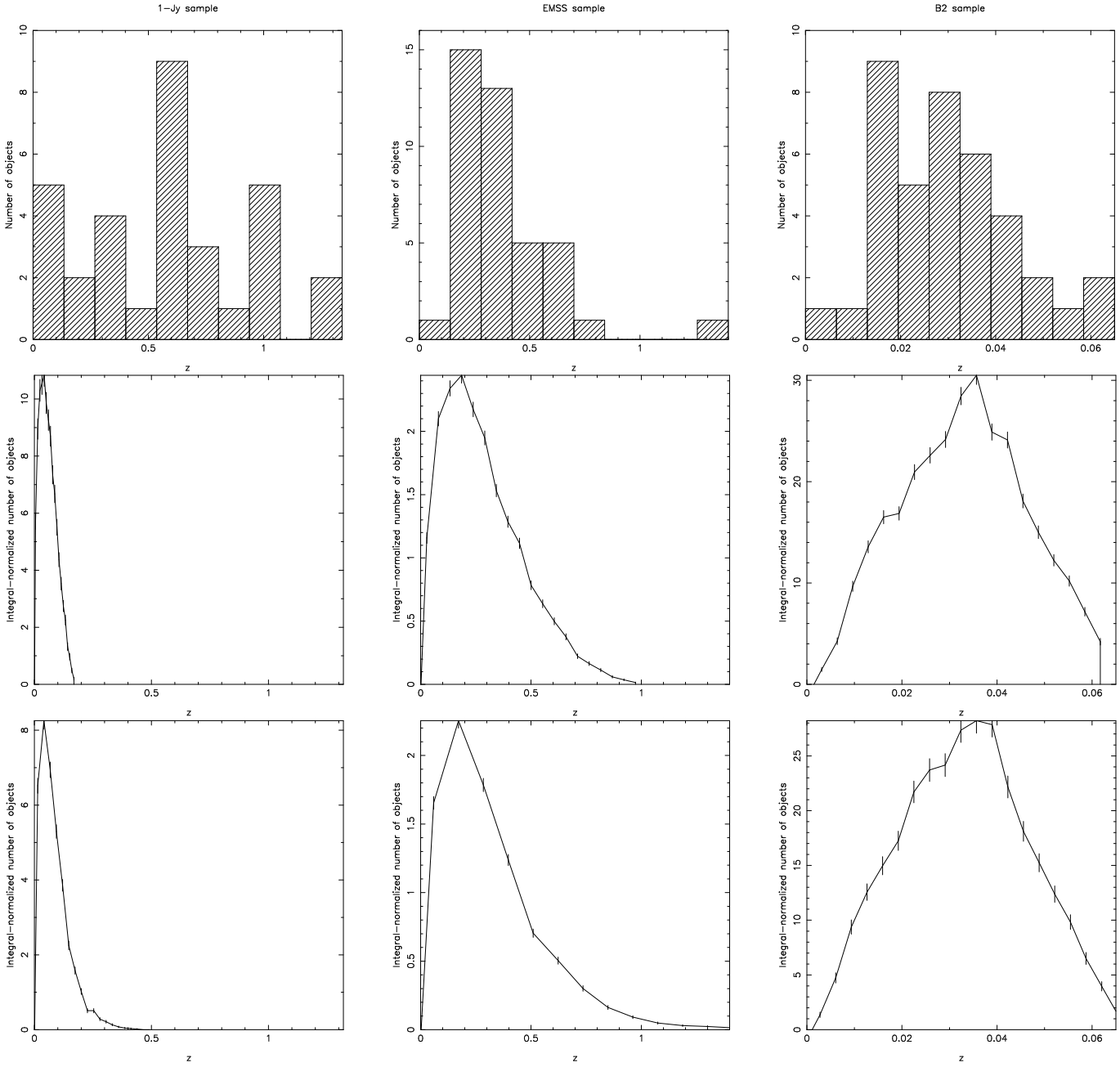

Figure 6. Redshift distributions for the real and simulated samples. Top: the real redshift distribution for the BL Lac and radio-galaxy samples, including BL Lacs without determined redshifts, which are assigned the median value. Middle: the distribution for simulated samples with $\gamma = 3.5$. The EMSS sample is reasonably well matched by the simulations, but there are no high-redshift 1-Jy objects. Bottom: the distribution of simulated samples with $\gamma = 3.0$ and 0.4 dex of dispersion in the intrinsic radio-X-ray relation. Simulated distributions are plotted with normalization such that the integral under the curve is unity; see Table 2 for the mean number of sources in these models. Note that a much smaller redshift range is plotted for the B2 sources than for the other objects.

5.4 The difference between X-ray and radio-selected samples

5.4.1 Dispersion in the intrinsic radio-X-ray relation

A simple way of producing a distinction between the two BL Lac samples is to assume that there is some dispersion, uncorrelated with intrinsic luminosity, in the intrinsic (rest-frame) relationship between X-ray and radio core flux, reflecting source-to-source variation in, for example, the structure of the jet or the size and age of the extended emission. This is distinct from, but in practice has very similar effects to, introducing an uncorrelated dispersion in the beaming Lorentz factors for the radio and X-ray components. Since the most luminous sources at any given redshift are most likely to be selected, we expect sources selected in the radio to be typically more radio-luminous than sources in the X-ray, and vice versa. We can use our simulations to investigate how great this dispersion should be. A starting point is the estimated logarithmic dispersion about the regression line in the radio-galaxy radio-X-ray core luminosity relationship (Canosa et al. 1999), which was about 0.2 decades. This is an underestimate of the dispersion in the *rest-frame* relationship, because common correlation of the X-ray and

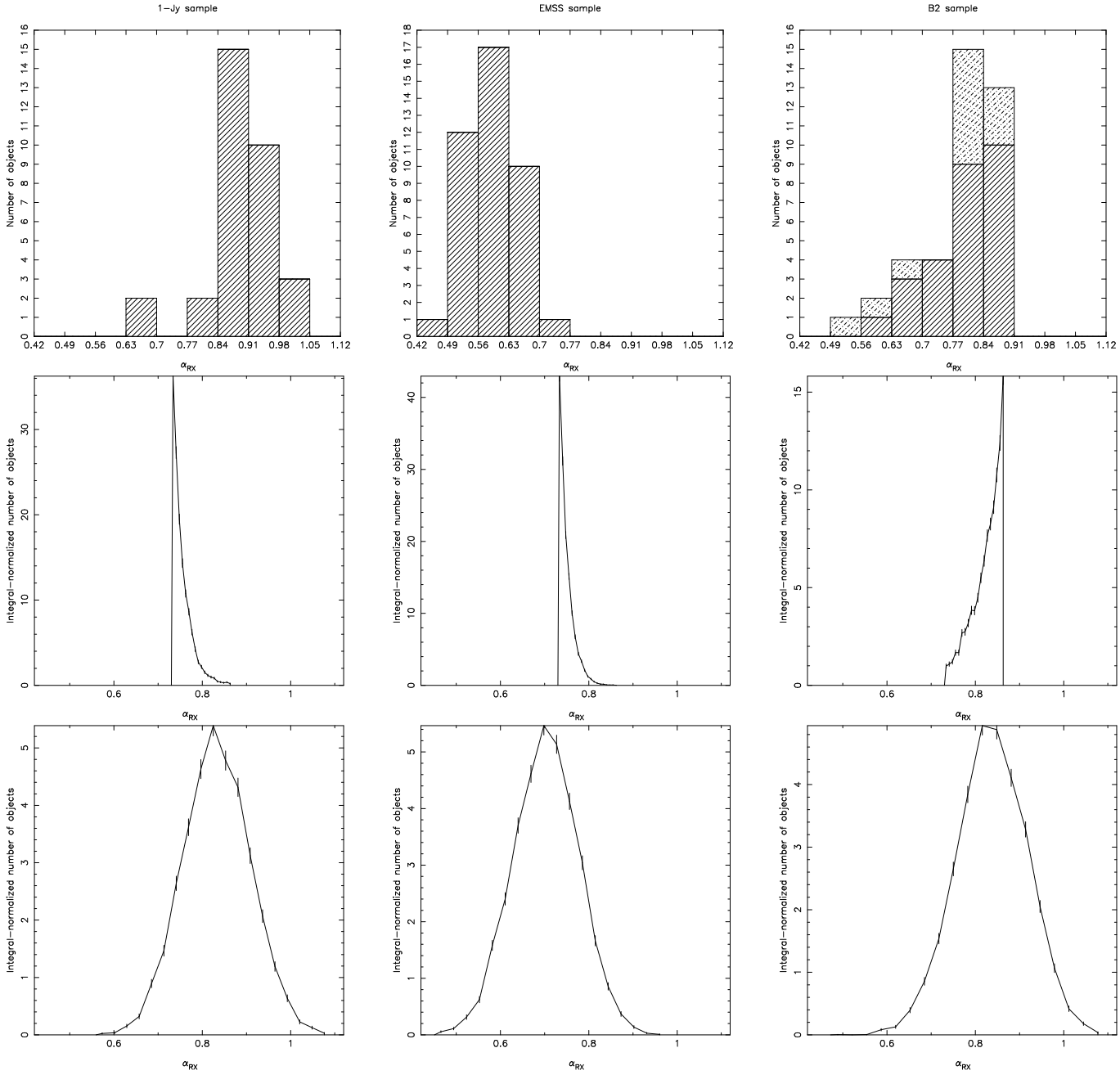

Figure 7. Distribution of the radio-X-ray spectral index ($\alpha_{\rm RX}$) for the three samples: 1-Jy BL Lac objects (left), EMSS BL Lacs (centre) and B2 radio galaxies (right). Top: the real distribution (dashed boxes indicate lower limits on $\alpha_{\rm RX}$). Middle: the distribution for simulated samples with no dispersion in the radio-X-ray relation and $\gamma = 3.5$. The small dispersion in observed $\alpha_{\rm RX}$ arises as a result of the different spectral indices assumed for radio and X-ray bands in the Doppler beaming calculation. The simulations clearly do not match the data. Bottom: the distribution of simulated samples with $\gamma = 3.0$ and 0.4 dex of dispersion in the rest-frame ratio of core X-ray to core radio luminosity. This comes much closer to the observed results. Simulated distributions are plotted with normalization such that the integral under the curve is unity; see Table 2 for the mean number of sources in these models.

radio core luminosities with the intrinsic luminosity of the source tends to stretch out the observed correlation. But even 0.2 dex of dispersion begins to recover the differences between the luminosity functions of the two BL Lac samples. Larger dispersions produce larger differences between the slopes of the luminosity functions and the distributions of $\alpha_{\rm RX}$, but also produce more sources (Table 2). The models which come closest to satisfying criteria (i), (ii) and (iv) above for the radio luminosity function seem to be those which combine a low γ with a moderate dispersion; the luminosity functions for a representative model, with $\gamma = 3.0$ and a dispersion of 0.4 dex in the intrinsic radio-X-ray relation, are plotted in Fig. 8 (compare Fig. 2) and the distribution of spectral indices for this model is plotted in Fig. 7. These models also replicate reasonably well the slope and range of the X-ray luminosity function for the simulated EMSS sample. However, we are not able to reproduce the observed steep slope of the 1-Jy X-ray luminosity function (Fig. 3).

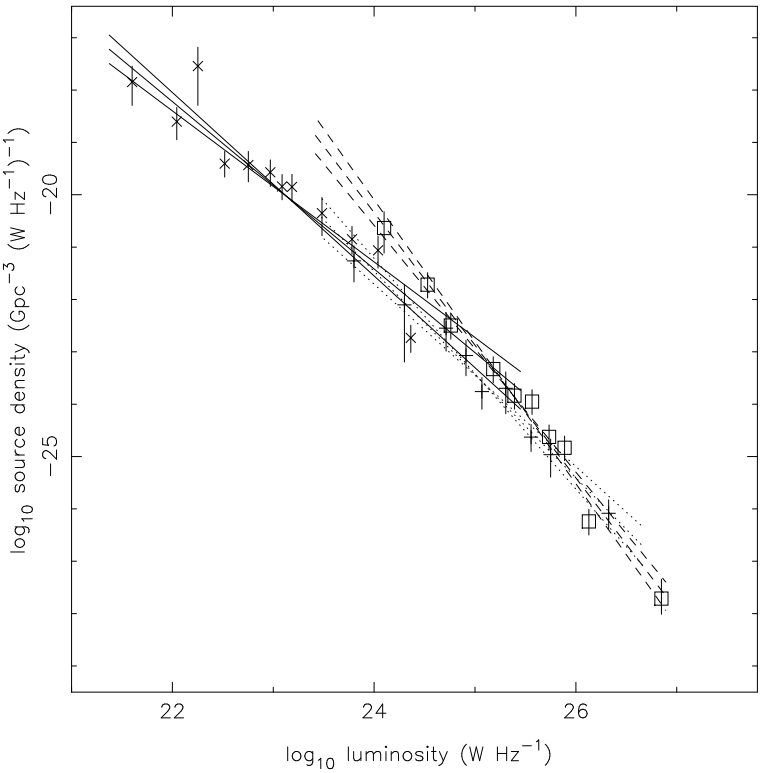

Figure 8. Simulated 5-GHz luminosity function for B2 radio galaxies, 1-Jy BL Lac objects and EMSS BL Lac objects with $\gamma = 3.0$ and logarithmic dispersion of 0.4 dex (1σ) in the intrinsic ratio of radio and X-ray cores to extended luminosity. The symbols and scale match those of Fig. 2. Differences between the luminosity functions of the two BL Lac populations are evident, as in the real data. This model also predicts approximately the right numbers of sources.

5.4.2 Asymmetrical dispersion

It is of interest to ask whether an asymmetrical dispersion in the radio-X-ray relationship can reproduce the observations in the same way. This would correspond to the situation in which the radio-selected objects are the tail of a population of X-ray-dominant objects, or vice versa. We investigated this by allowing either the radio or the X-ray intrinsic prominence to have a dispersion of 0.5 dex (1σ) above the mean values determined from the radio galaxies; this corresponds to radio-dominance or X-ray-dominance. Unsurprisingly, such models do not reproduce the difference between the luminosity functions in both bands; for example, if the X-rays have no dispersion in intrinsic prominence, then we see little difference between the X-ray luminosity functions of radio-selected and X-ray-selected objects, although their radio luminosity functions are different. We need dispersion in both bands to reproduce the differences in their luminosity functions.

5.4.3 Different Lorentz factors

It has been suggested (section 1) that the differences between X-ray and radio-selected objects can be attributed to different Lorentz factors for the regions emitting in the two wavebands. Our simulations show that the observed correlation between X-ray and radio core luminosity for the B2 objects (Canosa et al. 1999) is not consistent with isotropic X-ray emission, but we cannot rule out models in which the X-ray nuclei are beamed with a Lorentz factor considerably lower than that of the radio, as has been proposed to account for the less extreme properties of X-ray selected objects. Values of $\gamma_{\rm Xray} \lesssim 3$ do not produce enough EMSS BL Lacs in our model; if the Lorentz factors were this low, then these sources would have to have a different parent population. With $\gamma_{\rm Xray} = 3$, $\gamma_{\rm radio} = 5$ we do not see any significant difference between the slopes or normalizations of the populations in the two samples. Different Lorentz factors cannot alone be responsible for the difference in the observed luminosity function slopes and normalizations, although, by the same token, we cannot use the observed luminosity functions to rule out mildly differing Lorentz factors, since intrinsic dispersion in the radio-X-ray relation would obscure their effects.

5.4.4 Luminosity dependence of $\alpha_{\rm RX}$

A further way to try to reproduce the difference between the radio- and X-ray-selected BL Lac samples would be to include some luminosity dependence into the X-ray/radio relationship, as described by Fossati et al. (1998). The simplest way to parametrise this would be in terms of an α_{RX} which varies with luminosity. Unfortunately, the correlations in Fossati et al. are parametrised in terms of 5-GHz luminosity, which is itself a beamed quantity; for our purposes we need some relation between the shape of the SED and the beam power as parametrised by the low-frequency unbeamed luminosity. To test whether this kind of model can reproduce the observed difference in the luminosity functions of the different samples, we made the intrinsic X-ray flux fraction a function of intrinsic 408-MHz luminosity, while keeping the intrinsic radio flux fraction constant. We chose a dependence on luminosity such that $\alpha_{\rm RX}$ increases linearly with luminosity, going from 0.6 in the least luminous sources to 1.0 in the most luminous sources we observed; this approximately matches the magnitude of the range in $\alpha_{\rm RX}$ seen by Fossati et al. (see, e.g., their figure 8), though over a considerably smaller range in radio luminosity. This has some un-

realistic effects – for example, because the majority of sources are low-luminosity and flat-spectrum, the model vastly overpredicts the number of X-ray-selected sources (Table 2) and also predicts an inconsistent $\alpha_{\rm RX}$ distribution. However, it does give rise to clear differences between the luminosity functions of the two simulated BL Lac samples, in the same sense as, though of smaller magnitude than, the differences seen in the data. We conclude that luminosity dependence of the X-ray/radio relationship is probably not in itself enough to explain the differences in the luminosity functions of the two populations.

6 SUMMARY AND DISCUSSION

In this paper we have been trying to determine to what extent and under what assumptions B2 radio galaxies (or, more accurately, the radio galaxy population represented by the B2 radio galaxies) can be the parent population of two well-studied samples of BL Lac objects (the EMSS and 1-Jy samples). Following earlier work, we have characterized the properties of the populations using their luminosity functions: luminosity functions for the B2 and BL Lac samples were constructed in sections 2 and 3. In section 4 we discussed the analytical results of Urry & Schafer (1984); we argued that their models cannot properly be applied to luminosity functions of samples with different selection criteria.

Instead, in sections 5.1 and 5.2, we used Monte Carlo simulations to set up a parent population of beamed radio galaxies with B2-like properties and drew objects from them with selection criteria which as closely as possible matched those actually used in generating the EMSS and 1-Jy samples. By adjusting the unknown parameters of the simulation (section 5.3) we were able to show that our simulated observations of a beamed population of radio galaxies matched to the B2 sample were able to reproduce reasonably well the observed numbers of BL Lac objects and the slopes of the radio- and X-ray-selected BL Lac luminosity functions, if low values (~ 3) of the beaming Lorentz factor γ are adopted. In section 5.4.1 we found that the introduction of a moderate dispersion in the rest-frame ratio of core X-ray to core radio luminosity (for which there is some direct evidence in the observations of the B2 radio galaxies) can help to explain the observed differences in the luminosity functions and radio-to-X-ray spectral indices of radio-selected and X-ray-selected BL Lacs. This approach gives better results than other proposed ways of generating the differences between BL Lac populations (sections 5.4.2 – 5.4.4). These results therefore support a model in which the two apparently different BL Lac populations are simply extreme objects drawn from a single parent population (cf. Laurent-Muehleisen et al. 1999), although we have not attempted to reproduce all of the observed differences between radio-selected and X-ray-selected BL Lacs, such as the apparent differences in cosmological evolution (section 1).

The beaming Lorentz factors used here are much smaller than those inferred from superluminal motion or γ-ray transparency in some BL Lac objects. These typically require $\gamma \gtrsim 10$, which would grossly overpredict the number of BL Lac objects that should be observed above the flux limit (cf. Table 2). Chiaberge et al. (2000) have previously pointed out that the nuclear luminosities of FRI radio galaxies are a factor 10–10^4 too bright to be consistent with the 'de-beaming' of BL Lacs using these high Lorentz factors. The solution they adopt, velocity structure in the nuclear jet, seems plausible in view of what we know about the existence of velocity-structures in the *kiloparsec*-scale jets (e.g., Laing 1996). Velocity structure in the jets should not significantly affect our general conclusions here. If jets have velocity structure, our values of γ parametrize the relationship between the observed luminosity and the angle to the line of sight, rather than describing real physical bulk velocities. However, the details of this parameterization make a difference to the predicted numbers of BL Lac objects and the range in their luminosities. Although attempting to determine a typical jet emissivity/velocity profile is beyond the scope of this paper, it is certainly the case that luminosity functions can be used to help to constrain it.

The simulated observations fail to reproduce the real data in two important ways. Firstly, although the simulated EMSS sample is a good match in redshift distribution to the observed objects (Fig. 6, the simulated 1-Jy sample contains far too few high-redshift objects. As discussed in section 1, the EMSS objects seem all to be FRI-like in their radio structure and luminosity, while it is known that some 1-Jy objects are FRII-like; since FRIIs have higher luminosities than the parent population we use, it is not surprising that some of the 1-Jy sample appear at higher redshifts. Our models predict that essentially all the 1-Jy objects whose parent population are FRIs should have redshifts less than ~ 0.55 (Fig. 6), which agrees well with the observations of Rector & Stocke (2001). The fact that some of the 1-Jy objects may have a different parent population may also help to explain the anomalously steep 1-Jy X-ray luminosity function.

Secondly, the simulations predict a considerably larger number of BL Lac objects than is observed (by factors $\gtrsim 2$) for $\gamma \gtrsim 4$ or if a significant dispersion in intrinsic $\alpha_{\rm RX}$ is introduced; even the models which best reproduce other features of the population, such as the differences between the slopes of the X-ray and radio luminosity functions, overpredict the numbers of 1-Jy BL Lacs by a factor ~ 1.5. The mismatch in numbers becomes even greater if some of the observed high-redshift 1-Jy objects are not drawn from an FRI parent population, as discussed above. We can attribute at least some of this effect to the optical selection criteria applied when defining BL Lac samples. As pointed out by Marchã et al. (1996), a definition in terms of the strength of the 4000-Å break measures the strength of the optical non-thermal emission in terms of the starlight in the host galaxy, which may have very little to do with the AGN, while a condition on the equivalent width of the strongest emission lines has little physical justification (and may exclude objects which are in all other ways BL Lac objects; cf. Vermeulen et al. 1995). So some of the predicted objects may be present in the surveys, identified as something other than BL Lacs. However, a search in the EMSS survey for objects intermediate between FRIs and traditional EMSS BL Lacs (Rector et al. 1999) found relatively few candidates, and only a handful of EMSS sources are directly identified with radio galaxies. It remains possible that some of our simulated sources are identified as groups or clusters in the EMSS survey. If, as new *Chandra* results (section 1) suggest, we are overestimating the radio galaxies' nuclear X-ray fluxes (section 1) then we will also have overestimated the intrinsic X-ray core prominence; correcting for this would result in a (probably small) reduction in the predicted total number of EMSS sources. In the 1-Jy sample, there are additional optical magnitude and radio spectral selection criteria which are not modelled in our simulations, and so there is more scope for 'hiding' the excess sources. On the other hand, we are extrapolating our B2 luminosity function to high redshifts to generate BL Lac objects without including the effects of cosmological evolution of the FRI population, now reasonably well-established (e.g., Waddington et al. 2001). Because there is little evidence for evolution below $z < 0.5$, where most of our BL Lac candidates are generated (Fig. 6), this does not have a strong

effect on our models, but there may be up to an order of magnitude increase in the numbers of the most luminous sources at $z \sim 1$. Taking this into account would lead our models to produce ~ 10 additional high-redshift 1-Jy objects. Without a detailed model for source evolution, we cannot make this more quantitative.

Combining these factors with the large statistical uncertainties on the predicted and actual numbers of objects, we regard the degree of agreement between the simulations and observations as encouraging. It supports a model in which FRI radio galaxies in the luminosity range of the B2 bright sample are the parent population of all the EMSS X-ray-selected BL Lac objects, and of ~ 50 per cent of the radio-selected 1-Jy objects. A higher-luminosity population, probably beamed FRIIs, must be responsible for the remaining, higher-redshift, 1-Jy objects.

ACKNOWLEDGEMENTS

We are grateful for support from NASA grant NAG 5-1882 and from PPARC. CMC thanks the University of Bristol for a research studentship.

REFERENCES

Abraham, R.G., McHardy, I.M., Crawford, C.S., 1991, MNRAS, 252, 482
Antonucci, R.R.J., Ulvestad, J.S., 1985, ApJ, 294, 158
Baars, J.W.M., Genzel, R., Pauliny-Toth, I.I.K., Witzel, A., 1977, A&A, 61, 99
Browne, I.W.A., 1983, MNRAS, 204, 23p
Canosa, C.M., Worrall, D.M., Hardcastle, M.J., Birkinshaw, M., 1999, MNRAS, 310, 30
Celotti, A., Maraschi, L., Ghisellini, G., Caccianiga, A., Maccacaro, T., 1993, ApJ, 416, 118
Chiaberge, M., Celotti, A., Capetti, A., Ghisellini, G., 2000, A&A, 358, 104
Colla, G., et al., 1970, A&AS, 1, 281
Colla, G., Fanti, C., Fanti, R., Gioia, I., Lari, C., Lequeux, J., Lucas, R., Ulrich, M.H., 1975, A&AS, 20, 1
Condon, J.J., 1989, ApJ, 338, 13
Cotton, W.D., Ferretti, L., Giovannini, G., Venturi, T., Lara, L., Marcaide, J., Wehrle, A.E., 1995, ApJ, 452, 605
Fabbiano, G., Miller, L., Trinchieri, G., Longair, M., Elvis, M., 1984, ApJ, 277, 115
Falomo, R., 1996, MNRAS, 283, 241
Fanti, C., Fanti, R., De Ruiter, H.R., Parma, P., 1987, A&AS, 69, 57
Fossati, G., Celotti, A., Ghisellini, G., Maraschi, L., 1997, MNRAS, 289, 136
Fossati, G., Maraschi, L., Celotti, A., Comastri, A., Ghisellini, G., 1998, MNRAS, 299, 433
Ghisellini, G., Maraschi, L., 1989, ApJ, 340, 181
Giommi, P., Padovani, P., 1994, MNRAS, 268, 51
Giovannini, G., Feretti, L., Gregorini, L., Parma, P., 1988, A&A, 199, 73
Giovannini, G., Taylor, G.B., Arbizzani, E., Bondi, M., Cotton, W.D., Feretti, L., Lara, L., Venturi, T., 1999, ApJ, 522, 101
Hardcastle, M.J., Alexander, P., Pooley, G.G., Riley, J.M., 1999, MNRAS, 304, 135
Hardcastle, M.J., Worrall, D.M., 1999, MNRAS, 309, 969
Hardcastle, M.J., Worrall, D.M., 2000, MNRAS, 314, 359
Hardcastle, M.J., Worrall, D.M., Birkinshaw, M., Laing, R.A., Bridle, A.H., 2002, MNRAS, 334, 182
Jannuzi, B.T., Smith, P.S., Elston, R., 1994, ApJ, 428, 130
Kellermann, K.I., 1964, AJ, 69, 205
Kollgaard, R.I., Wardle, J.F.C., Roberts, D.H., Gabuzda, D.C., 1992, AJ, 104, 1687
Laing, R.A., 1996, in Hardee P.E., Bridle A.H., Zensus J.A., eds, Energy Transport in Radio Galaxies and Quasars, ASP Conference Series vol. 100, San Francisco, p. 241
Laing, R.A., Parma, P., de Ruiter H.R., Fanti, R., 1999, MNRAS, 306, 513
Laurent-Muehleisen, S.A., Kollgaard, R.I., Moellenbrock, G.A., Feigelson, E.D., 1993, AJ, 106, 875
Laurent-Muehleisen, S.A., Kollgaard, R.I., Feigelson, E.D., Brinkmann, W., Siebert, J., 1999, ApJ, 525, 127
Machalski, J., Godlowski, W., 2000, A&A, 360, 463
Maraschi, L., Ghisellini, G., Tanzi, E.G., Treves, A., 1986, ApJ, 310, 325
Marchã, M.J.M., Browne, I.W.A., Impey, C.D., Smith, P.S., 1996, MNRAS, 281, 425
Morganti, R., Oosterloo, T.A., Fosbury, R.A.E., Tadhunter, C.N., 1995, MNRAS, 274, 393
Morris, S.L., Stocke, J.T., Gioia, I.M., Schild, R.E., Wolter, A., Maccacaro, T., della Ceca R., 1991, ApJ, 380, 49
Padovani, P., Giommi, P., 1995, ApJ, 444, 567
Padovani, P., Urry, C.M., 1990, ApJ, 356, 75
Padovani, P., Urry, C.M., 1991, ApJ, 368, 373
Perlman, E.S., Stocke, J.T., 1993, ApJ, 406, 430
Perlman, E.S., Stocke, J.T., 1994, AJ, 106, 56
Pesce, J.E., Falomo, R., Treves, A., 1995, AJ, 110, 1554
Rector, T.A., Stocke, J.T., Perlman, E.S., Morris, S.L., Gioia, I.M., 2000, AJ, 120, 1626
Rector, T.A., Stocke, J.T., 2001, AJ in press [astro-ph/0105100]
Sadler, E.M., et al., 2001, MNRAS submitted, astro-ph/0106173
Sambruna, R.M., Maraschi, L., Urry, C.M., 1996, ApJ, 463, 444
Smith, E.P., O'Dea, C.P., Baum, S.A., 1995, ApJ, 441, 113
Stickel, M., Padovani, P., Urry, C.M., Fried, J.W., Kühr, H., 1991, ApJ, 374, 431
Stocke, J.T., Liebert, J., Schmidt, G., Gioia, I.M., Maccacaro, T., Schild, R.E., Maccagni, D., Arp, H.C., 1985, ApJ, 298, 619
Trussoni, E., Massaglia, S., Ferrari, R., Fanti, R., Feretti, L., Parma, P., Brinkmann, W., 1997, A&A, 327, 27
Ulrich, M.-H., 1989, in Maraschi L., Maccacaro T., Ulrich M.-H., eds, BL Lac objects, Springer-Verlag, Heidelberg, p. 47
Urry, C.M., Padovani, P., 1991, ApJ, 371, 60
Urry, C.M., Padovani, P., 1995, PASP, 107, 803
Urry, C.M., Padovani, P., Stickel, M., 1991, ApJ, 382, 501
Urry, C.M., Schafer, R.A., 1984, ApJ, 280, 569
Urry, C.M., Sambruna, R.M., Worrall, D.M., Kollgaard, R.I., Feigelson, E.D., Perlman, E.S., Stocke, J.T., 1996, ApJ, 463, 424
Venturi, T., Feretti, L., Giovannini, G., Comoretto, G., Wehrle, A.E., 1993, ApJ, 408, 81
Vermeulen, R.C., Ogle, P.M., Tran, H.D., Browne, I.W.A., Cohen, M.H., Readhead, A.C.S., Taylor, G.B., Goodrich, R.W., 1995, ApJ, 452, L5
Waddington, I., Dunlop, J.S., Peacock, J.A., Windhorst, R.A., 2001, MNRAS submitted (astro-ph/0108048)
Wall, J.V., Peacock, J.A., 1985, MNRAS, 216, 173
Wolter, A., Gioia, I.M., Maccacaro, T., Morris, S.L., Stocke, J.T., 1991, ApJ, 369, 314
Wolter, A., Caccaniga, A., della Ceca R., Maccacaro, T., 1994, ApJ, 433, 29
Worrall, D.M., Birkinshaw, M., 2000, ApJ, 530, 719
Worrall, D.M., Birkinshaw, M., Hardcastle, M.J., 2001, MNRAS, 326, L7
Wurtz, R., Stocke, J.T., Yee, M.K.C., 1996, ApJS, 103, 109
Wurtz, R., Stocke, J.T., Ellingson, E., 1997, ApJ, 480, 547

This paper has been typeset from a TEX/ LATEX file prepared by the author.